FOREX Publication
Open Access | Rapid and quality publishing

International Journal of Electrical and Electronics Research (IJEER)
Research Article | Volume 11, Issue 1 | Pages 01-09 | e-ISSN: 2347-470X

An efficient Feed-forward compensation mechanism for NFC-based PMSM system using different observers for Load-torque estimation

Parvathy Thampi M.S[1*] and G. Raghavendra N[2]

[1]*Assistant Professor, Department of EEE, CMRIT, Bengaluru, India; parvathy.t@cmrit.ac.in*
[2]*Associate Professor, Department of EEE, SEC, Bengaluru, India; raghavendrag@sapthagiri.edu.in*

***Correspondence:** Parvathy Thampi M.S, Email: parvathy.t@cmrit.ac.in*

ABSTRACT- Permanent magnet synchronous motor (PMSM) offers high torque and efficiency and is used in most industrial applications. This manuscript uses a feed-forward compensation mechanism to design an efficient neuro-fuzzy logic controller (NFC) based surface-mounted PMSM system. The different load-observers like Discrete Luenberger Observer (DLO), Kalman filter observer (KFO), and discrete Kalman filter observer (DKFO) are used as a feed-forward compensation method to compensate the *dq* stator current and also estimate performance metrics. The NFC is used as a speed controller, and two PI controllers are used for the current control mechanism. The noise is added at the actual load torque and speed of PMSM and compensated using load observers. In this work, two different design scenarios are considered to analyze the performance metrics like load torque, speed, and position. The work also explores the average error that occurred at load torque, speed, and position during estimation. The NFC-based PMSM system improves the performance and utilizes less error over the PI/FLC-based PMSM using different observers.

Keywords: Compensation; PMSM; Load-torque estimation; NFC; FLC.

ARTICLE INFORMATION

Author(s): Parvathy Thampi M.S and G. Raghavendra N;
Received: 08/10/2022; **Accepted**: 28/12/2022; **Published**: 30/01/2023;
e-ISSN: 2347-470X;
Paper Id: IJEER 0810-01;
Citation: 10.37391/IJEER.110101
Webpage-link:
www.ijeer.forexjournal.co.in/archive/volume-11/ijeer-110101.html

Publisher's Note: FOREX Publication stays neutral with regard to Jurisdictional claims in Published maps and institutional affiliations.

1. INTRODUCTION

The Permanent magnet synchronous motor (PMSM) offers high efficiency and torque density-based features, among other electrical-based machines. Recently, AC drives based on PMSM with brushless features have been used in most industrial applications, including renewable energy production and industrial drives. Most renewable energy resources use advanced technology concerning electrical machines, especially PMSM with AC drives to enhance energy security issues and environmental pollution. The rotor-mounted permanent magnet (PM) is an alternative to conventional synchronous machines due to its robustness and high torque features [1-2]. The AC drive-enabled PMSM offers low cost, high reliability, flexibility, high efficiency, high torque or power density, and good controllability features to run electrical applications smoothly. There are three types of stator-based PM machines based on the location of PMs: Flux switching, flux reversal, and doubly salient-based PM machines. The Flux switching PM machine (FSPM) improves the transient and steady-state performance of the other two PM machines. However, due to economic issues, FSPMs are replaced with rotor-based PMSMs [3].

The PMSMs are classified based on rotor shape, including spoke type, interior buried (IPMSM), and Surface mounted based (SPMSM). The PMSM drivers generally are closed-loop systems using a vector control mechanism. The field-orientated control (FOC) is one vector control approach that produces the torque and flux using transformation (*abc* to *dq*-axis). There are two types of PMSM parameter estimation approaches offline and online. The offline estimation has AC standstill, vector control, and DC decay test approaches. In contrast, the online estimation has Artificial Neural Network (ANN), model reference adaptive system (MRAS), Recursive Least Square (RLS), and Extended Kalman Filter (EKF) based approaches [4-5]. The PMSM system produces mainly load torque, speed, position, three-phase stator current, and *dq*-stator current parameters. The load-torque estimation is achieved using online estimation approaches, including unscented Kalman filter (UKF) and EKF in sensor less PMSM drives. The UKF and EKF are used to measure PMSM current to estimate performance metrics [6-7]. The sensor less IPMSM drives estimate the rotor position by detecting the *dq* stator currents using the pulse-width modulation (PWM) switching approach [8]. The IPMSM system estimates the load torque using reference voltage correction and a low-pass filter (LPF) as a compensation approach [9]. The Disturbance observer-based control (DOBC) is introduced to estimate the load torque and position in the IPMSM system [10].

An efficient feed-forward compensation mechanism for NFC based sensor less Surface mounted PMSM system is modeled using different load-torque observers to estimate the

FOREX Publication
Open Access | Rapid and quality publishing
International Journal of Electrical and Electronics Research (IJEER)
Research Article | Volume 11, Issue 1 | Pages 01-09 | e-ISSN: 2347-470X

performance metrics in this manuscript. The contribution of the work is listed as follows:

- The feed-forward compensation mechanism is used to estimate the performance metrics (torque load, speed, and position) using three load observers like Discrete Luenberger Observer (DLO), Kalman Filter Observer (KFO), and Discrete Kalman Filter Observer (DKFO).
- Two design scenarios are considered, including (1) fixed reference speed and variable torque load and (2) variable reference speed and variable torque load, to analyze the performance metrics.
- The work analyzes the average load-torque error, speed error, and position error by concerning the load observer's estimation. The work also compares the performance metrics and errors using different controllers (PI, FLC, and NFC) and observers.

The manuscript is organized as follows: *Section 2* describes the existing works of the PMSM system using different approaches to improve the performance metrics. The NFC-based PMSM system is discussed in *section 3*, including modeling, load-observers, and NFC operation. The simulation results are discussed in *section 4*, followed by a discussion in *section 5*. Lastly, it concludes the overall work with futuristic scope in *section 6*.

2. SYSTEM MODEL

This section discusses the existing works of the PMSM system with control mechanisms to improve the performance metrics. Zhao et al. [11] present an accurate torque control method with sensor less features for interior PMSM machines using a cascaded sliding mode observer (SMO). The work analysis the interior PMSM model, including αβ frame, *dq* frame, and active flux model with mathematical equations. The variable gain adaptive SMO controls the sensor less PMSM model and estimates the flux and torque. Tami et al. [12] describe an extended observer form-based PMSM to calculate the rotor speed, load torque, and position. The extended dynamics and coordinate changes are discussed in theorems. The adaptive observer via coordinate transformations is implemented to estimate the performance parameters. Asseu et al. [13] present the extended Kalman filter (EKF) for PMSM drive with experimental analysis. The real-time experimental setup is constructed with an ASIC interface and DSP-based control algorithm with the observer. The work analyzed the presence and absence of toque load concerning the speed, position, error position, and stator currents. Yang et al. [14] discuss the multipurpose disturbance observer for PMSM drive with the deadbeat predictive control (DBPC) mechanism. The work analyzed the disturbance estimation using an SM disturbance observer (SMDO) and deadbeat current control mechanism to estimate the position and robustness test.

Tian et al. [15] describe the EKF-based sensor less PMSM to estimate the rotor position. The work describes the PMSM mathematical model followed by a rotor position estimation algorithm using EKF. The yield forecast the speed, position, and stator current at different reference speed scenarios. Sun et al. [16] present the PMSM model with unknown load torque using an adaptive backstepping control mechanism. The adaptive backstepping control mechanism estimates the unknown load torque and improves the convergence speed. The control method also enhances the tracking position and stability of the PMSM drive. Zhang et al. [17] discuss the comparative study of the IPMSM concerning the inverter, regulators, and observer under low-switching frequency mode. Non-Singular terminal sliding mode (NTSM) and Fast NTSM theory design the regulator and observer. The work analyzes the position observed error, inverter-based non-linearity compensation, and position and speed performance analysis. Xu et al. [18] describe the SMO-based sensor less PMSM drive equipped with an LC filter. The inverter is connected with current sensors, followed by an LC filter to combine the PMSM drive. The work analyzed the speed, torque, and position in different design scenarios. Eldigair et al. [19] present the discrete-time SMC (DTSMC) based sensor less PMSM with the three-level inverter. The three-level DTSMC improves the control mechanism over maximum switching frequency. The DTSMC is used to control the speed of the PMSM drive.

Niewiara et al. [20] discuss the EKF-based PMSM to estimate the reduction of velocity ripples and periodic disturbances. The state feedback controller (SFC) is used to compensate for the disturbances in a feed-forward way. The disturbance estimation algorithm uses EKF to analyze the total harmonic distortion (THD) for rotational speed. Niedermayr et al. [21] present the sensor less control-based high-speed PMSM using EKF. The EKF estimates the position, speed, and three-phase current in the PMSM drive. Ge et al. [22] describe the sensor less PMSM using an adaptive resistance estimator and back EMF observer. The work analyzed the three-phase current, position, and back EMF at different speed scenarios. He et al. [23] present the SMO-based PMSM drive with a sensor less control mechanism. The work uses the extended electromotive force (EEMF) model of PMSM to realize the αβ and *dq* frames. The work analyzed the position error and speed errors at different reference speeds. Dilys et al. [24] discuss the EKF for PMSM drive with a sensor less control mechanism using an M3 microcontroller. The work improves the execution time of the EKF estimator with better accuracy. Wang et al. [25] describe the Fuzzy adaptive super-twisting (FAST) algorithm-based SMO for PMSM systems with a sensor less control mechanism. The work suppresses the chattering using SMO and improves the convergence speed using FAST-SMO in PMSM at variable speed and torque. Ye et al. [26] present the improved sensor less control-based PMSM using Fuzzy-PI-Phase locked-loop-based full-order SMO (FOSMO). The FLC improves the boundary–layer thickness to estimate error. The PLL adjusts the bandwidth with the integration of the PI controller.

In this work, The DLO and KFO are traditional observers and are used only for performance comparison purposes with DKFO. The computational complexity is more in Extended Kalman filters than in Discrete KFO. The proposed NFC requires less computational time for NN training than artificial neural network (ANN) based designs. The NFC combines the neural network and fuzzy logic-based controller, which

FOREX Publication
Open Access | Rapid and quality publishing
International Journal of Electrical and Electronics Research (IJEER)
Research Article | Volume 11, Issue 1 | Pages 01-09 | e-ISSN: 2347-470X

improves the system response more than traditional PI and FLC-based designs.

3. NFC-based PMSM System

The NFC-based PMSM system is designed using load torque observers, as shown in *figure 1*. It mainly contains NFC based speed controller, PI-based two Current controller, Back EMF decoupling unit, vector transformations, PMSM model, and different load observers. First, define the reference speed (W_{ref}) and load torque (T_l) values to initiate the PMSM system. The NFC-based PMSM system operates only after the synchronous motor produces the rotor angle (θ) and 3-phase stator current (I_{abc}). The abc to dq transformation is performed and has the 2-level measured stator currents (I_{dm} and I_{qm}). The measured stator current (I_{dm}) acts as a flux current, and the measured stator current (I_{qm}) acts as a toque current. The stator currents (I_{dm} and I_{qm}) are controlled independently using PI current controllers in the PMSM system. The reference flux current (I_{dref}) is set to zero, and the NFC speed controller produces the reference torque current (I_{qref}).

The Load observers produced the compensated toque current (I_{qc}) and added it with reference torque current (I_{qref}), and the results are input to the 1st PI-based current controller. The second PI-based current controller receives the reference flux current (I_{dref}) difference with measured stator currents (I_{dm}) as input. These two PI-based current controllers produce 2-level stator voltages (V_d and V_q).

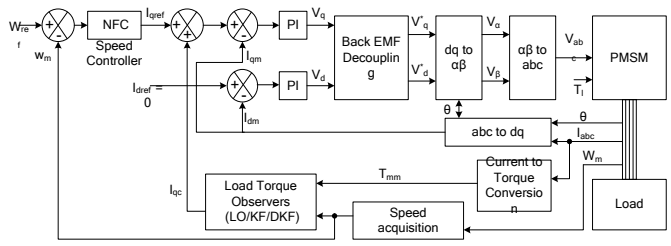

Figure 1: NFC-based PMSM system using load torque observers

The back EMF decoupling receives the 2-level stator voltage and makes the necessary three-phase voltages to the PMSM system via vector transformations. The back EMF decoupling has 2-level stator voltages (V_d and V_q), measured dq current ((I_{dm} and I_{qm}), and actual speed (W_m). It produces the 2-level command stator voltages to the vector transformation unit. These command stator voltages are essential in estimating the three-phase stator current in the PMSM system. The PMSM drive produces the three-phase stator current (I_{abc}), rotor angle (θ), actual speed (W_m), and electromagnetic torque (EMF). The measured stator currents (I_{dm} and I_{qm}) from the abc to dq transformation are added with noise, followed by electrical to torque conversion to generate measured load torque (Tmm). Similarly, actual speed (W_m) is added with noise, followed by electrical to mechanical conversion (1/4) to estimate speed. The measured load torque (T_{mm}) and estimating speed (wm) values are fed to load observers to produce the compensated toque current (I_{qc}) using a feed-forward compensation mechanism. The NFC receives the error signal, a difference between reference speeds (W_{ref}) and estimating speed (w_m). The following sections discuss a detailed explanation of PMSM modeling, feed-forward compensation mechanism using different load observers, and neuro-fuzzy controller (NFC).

3.1 PMSM Modeling

The Surface-mounted PMSM system is designed concerning this work's field-oriented control (FOC) mechanism. The FOC offers independent control features for torque and flux using transformation methods. The FOC is used in many motor control applications with configurable speed mechanisms. The permanent magnets are designated on the motor's Surface. The Surface-mounted PMSM is non-salient and offers equal motor inductance on the direct and quadrature *dq*-axis. The PMSM system is modeled with a few assumptions, like a number of turns is matched with stator winding and using two-phase *dq* axes. The PMSM drive is symmetric and uses balanced 3-phase voltages. The two-axis motor voltages concerning the stator winding are represented in *equations (1-2)* as follows:

$$V_q = I_q R_s + W_m \lambda_d + \rho \lambda_q \quad (1)$$

$$V_d = R_s I_d - W_m \lambda_q + \rho \lambda_d \quad (2)$$

The position of the motor flux linkages depends on the dq-axis reference (Stator) frame. The motor flux linkages in *equation (3)* for the *dq*-axis. So, the substitution of λ_d and λ_q values in *equations (1-2)* and the updated motor voltages are expressed in *equation (4-5)* as follows:

$$\lambda_d = I_d L_d + \lambda_f \text{ And } \lambda_q = I_q L_q \quad (3)$$

$$V_q = I_q R_s + W_m (I_d L_d + \lambda_f) + \rho (I_q L_q) \quad (4)$$

$$V_d = I_d R_s - W_m (I_q L_q) + \rho (I_d L_d + \lambda_f) \quad (5)$$

The 1st order differential equation for (4-5) is represented in *equations (6-7)*, and the above *dq* voltages *equations (4-5)* include the back EMF decoupling features and are expressed in *equation (8)* as follows:

$$\rho I_q = -I_q \left(\frac{R_s}{L_q}\right) - W_m I_d \left(\frac{L_d}{L_q}\right) - W_m \lambda_f \left(\frac{1}{L_q}\right) + V_q \left(\frac{1}{L_q}\right) \quad (6)$$

$$\rho I_d = -I_d \left(\frac{R_s}{L_d}\right) + W_m I_q \left(\frac{L_q}{L_d}\right) + V_d \left(\frac{1}{L_d}\right) \quad (7)$$

$$V_q^* = (I_d L_d + \lambda_f) \text{ And } V_d^* = -(L_q W_m I_q) \quad (8)$$

Notations: Winding resistance of the stator is (R_s), the Inductance of the dq-axis is (L_d & L_q), the dq-axis stator voltages are (Vd & Vq), dq-axis stator currents are (Id & Iq), Stator flux linkages (dq-axis) is (λ_d & λ_q), rotor magnets-based stator flux linkages is λ_f, the derivative operator is (ρ), Motor electric Speed is (W_m).

The electromagnetic Torque (EMT) measures the motor's position and rotor speed. The windings input power is calculated using the torque equation and is represented in *equation (9)*. Once the stator dq-current (I_{dm} and I_{qm}) is measured using stator current (I_{abc}) and theta (θ), then add noise to calculate the measured load torque (T_{mm}). The measured torque is governed after the current (electrical) to mechanical

FOREX Publication
Open Access | Rapid and quality publishing
International Journal of Electrical and Electronics Research (IJEER)
Research Article | Volume 11, Issue 1 | Pages 01-09 | e-ISSN: 2347-470X

conversion using *equation (10)*. The reluctance torque is measured using the $(I_{qm}\lambda_d - I_{dm}\lambda_q)$ difference and mutual reaction torque is measured using $(\lambda_f I_{qm})$. The mechanical torque is calculated using *equation (11)* per newton's 2nd law.

$$T_e = 1.5\, N_P\, (I_q\lambda_d - I_d\lambda_q) \quad (9)$$

$$T_{mm} = 1.5\, N_P \left(\left(I_{qm}\lambda_d - I_{dm}\lambda_q\right) + \lambda_f I_{qm}\right) + T_n \quad (10)$$

$$T_{em} = w_m B + J\frac{dw_m}{dt} + T_n \quad (11)$$

The 2nd term of *equation (11)* is modified, and it is equal to the summation of mechanical torque values (T_s), and the rotor's speed is $\dot{w}_m = \frac{1}{J}\sum T_s$. So inertial rotor speed is expressed in *equation (12)*. After the modification, the actuator's dynamics appear in 1st order, as represented in *equation (13)*.

$$J\dot{w}_m = T_{em} - T_l - w_m B - T_n \quad (12)$$

$$\dot{T}_{em} = \frac{1}{\tau_{em}}(T_e - T_{em}) \quad (13)$$

Notations: The number of pole pairs is (N_p), measured stator *dq*-currents are (I_{dm} and I_{qm}), the Mechanical based rotor's speed is (w_m), J is inertia, Viscous friction co-efficient is (B), disturbance Torque is (T_n), Torque load is (T_l) and Torque time constant is (τ_m).

3.2 State Observers

The state observer or estimator estimates the given system's internal state from the system's actual (measured) input and outputs. In this work, three different types of state estimators or observers are used, namely:
(1) Luenberger observer,
(2) Kalman filter (KF) and
(3)Discrete Kalman filter (DKF).
These state observers estimate real load torque/speed from measured and input torque/reference speed. The Luenberger observer is one of the traditional state observers and is used to estimate the load torque.

Luenberger observer: The mechanical torque is used to construct the load torque observers, and the state-space form for the Luenberger observer [27] of the system is represented in *equation (14)*. When torque is already transformed in the state, the estimated state-space for continuous Luenberger observer is represented in *equations (15 and 16)*:

$$\dot{m} = Pa + Qi + Hk \text{ And } n = Sa + Ui + j \quad (14)$$

$$\begin{pmatrix}\dot{w}_m \\ \dot{T}_l\end{pmatrix} = \begin{pmatrix}-(B/J) & -(1/J) \\ 0 & \tau_l\end{pmatrix}\begin{pmatrix}w_m \\ T_l\end{pmatrix} + \begin{pmatrix}1/J \\ 0\end{pmatrix} T_{em} + \begin{pmatrix}1 & 0 \\ 0 & 1\end{pmatrix}\begin{pmatrix}w_m \\ w_{mn}\end{pmatrix} \quad (15)$$

$$w_m = (1 \quad 0)\begin{pmatrix}w_m \\ T_l\end{pmatrix} + j_m \quad (16)$$

The U and τ_l are set to zero. The 2nd order system's observabillity matrix is represented as Obs = [S SP]. The system's matrix is observable and full rank. So continuous Luenberger observer is described in *equation (17)* as follows [27]:

$$\dot{\hat{m}} = P\hat{m} + Qi + L[n - (S\hat{m} + Ui)] = (P - LS)\hat{m} + [Q\ L]\begin{pmatrix}i \\ n\end{pmatrix} \text{ And } \dot{\hat{n}} = S\hat{m} \quad (17)$$

Using *equations (17)*, the system is stable (P-LS) using observers gains (L). The pole placement controlling mechanism is used to design the 'L.' The discrete Luenberger observer (DLO) is created by modifying *equation (17)* by concerning the observer gain (L). So DLO is represented in *equation (18)* as follows:

$$P_{es} = P - LS;\ Q_{es} = (Q \quad L);\ S_{es} = \begin{pmatrix}1 & 0 \\ 0 & 1\end{pmatrix};\ U_{es} = 0 \quad (18)$$

Discrete Kalman filter (KF): The Kalman filter (KF) is an arbitrary alternative to the Luenberger observer and is used in most electrical machines for controlling operations. The KF operates parallel with the PMSM system and offers the estimation of the linear system's states. The KF approach is used not to measure states in linear systems. The KF is optimal and estimates the uncorrelated and average estimation error. In the PMSM system. The KF is set to estimate the load toque and filter signal by concerning the measured speed after adding the noise. The discrete state-space form for the KF observer of the system is represented in *equation (19)* as below [28]:

$$\dot{m}_c = P_{c-1}m_{c-1} + Q_{c-1}i_{c-1} + k_{c-1} \text{ And } n_c = S_c m_c + j_c \quad (19)$$

The noises (processed and measured) are white, uncorrelated, and zero-mean (k_c, j_c) and appear in known covariance matrices (X and Y) respectively and are represented in *equation (20)* as follows:

$$E\left[k_c {k_d}^T\right] = X_c\delta_{c-d} \text{ And } E\left[j_c {j_d}^T\right] = Y_c\delta_{c-d} \text{ and } E\left[k_c {j_d}^T\right] = 0 \quad (20)$$

Where delta function ($\delta_{c\text{-}d}$) = 1 (when c = d) and 0 (when c ≠ d).

In the discrete Kalman filter (DKF), the first filter initializes by concerning the initial state a_0 to form the expected value ($\hat{m}_0$) and state estimation error (Z_0) and are represented in *equation (21)*. The propagated state estimate and updated state estimated error covariance matrices are described in *equation (22)*. Lastly, the KF gain is calculated using *equation (23)* [28]:

$$\hat{m}_0 = E(m_0) \text{ And } Z_0 = E(m_0 - \hat{m}_0)(m_0 - \hat{m}_0)^T \quad (21)$$

$$\hat{m}_c^1 = P_{c-1}\hat{m}_{c-1} + Q_{c-1}i_{c-1} \quad \text{And} \quad Z_c^1 = P_{c-1}Z_{c-1}P_{c-1}^T + X_{c-1} \quad (22)$$

$$KF_c = \frac{Z_c^1 S_C^T}{S_c Z_c^1 S_C^T + Y_c} \quad (23)$$

From *equation (23)*, the prior uncertainty is calculated from the numerator term, and measurement uncertainty is calculated from the denominator term. The Final state estimate (Correction step) and final updated state estimated error covariance matrices are represented in *equation (24)* as follows [28]:

FOREX Publication
Open Access | Rapid and quality publishing
International Journal of Electrical and Electronics Research (IJEER)
Research Article | Volume 11, Issue 1 | Pages 01-09 | e-ISSN: 2347-470X

$\hat{m}_c = \hat{m}_c^1 + KF_c\,(n_c - S_c\hat{m}_c^1)$ And $Z_c = (I - KF_c\,S_c)Z_c^1$ (24)

The overshoot time is reduced using the covariance matrix (Z_c) due to propagated state estimates (Z_c^1) is multiplied by the term (($I - KF_c\,S_c$) is less than 1. When the covariance matrices X_c increase or Y_c decreases, the Kalman filter gain will be increased based on Z_c^1 value.

3.3 Neuro-Fuzzy Controller (NFC)

The Neuro-Fuzzy Controller (NFC) is an extended version of FLC with an Artificial-neuro-fuzzy interface system (ANFIS). The Fuzzy interface system (FIS) realization is automatically achieved in NFC using neural networks (NNs). The NFC effectively transforms absolute values (Crisp) to fuzzy values and vice-versa by about the FIS. The neural network model is used in NFC to enhance the FIS and adopted in the ANFIS system. In general, the NFC performs four operations: training data, generation of FIS, training the FIS, and testing FIS against training data. The NN can train and test the input data using its own learning set. The representation of the NFC operation is shown in *figure 2*. The NFC receives an error signal for training. The difference between the reference speed and estimating speed generates the error signal and is considered training data in NFC. The NFC receives two input data: error data (Ei) and change in error data (CEi), and generates one output data (On). The two input data are used for training. Once training is done, load the training data for FIS generation. The FIS is generated based on a grid partition with triangle membership functions. The FIS is constructed using seven membership functions with a linear output type for FIS training. The FIS training is performed based hybrid approach (optimization) for FIS-generated data. The FIS training is completed with three epochs of error tolerance. Finally, test the trained FIS data against the input data to generate the NFC output.

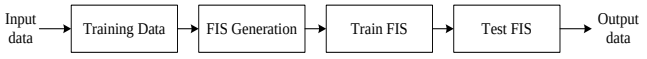

Figure 2: NFC operation

4. RESULTS

The NFC-based PMSM system uses different load-torque observers to estimate the load torque, speed, and position (angle). The complete work is modeled using MATLAB Simulink. The different load-torque observers like LO, KFO, and DKFO estimate the load-torque and provide the compensated feed-forward current to the current controller. The noise is added to both actual torque and speed to analyze the load observer's performance concerning the speed, load-toque, and position. The average error for load torque, speed, and position (angle) is based on the observers' estimation. The performance of the NFC-based PMSM system is compared with the PI and Fuzzy logic controllers (FLC) with better improvements. The specifications used in the PMSM modeling are tabulated in *table 1*. In this work, reference speed and torque load are considered two different design scenarios (C1 and C2). The design scenarios used for the PMSM system using load torque observers are tabulated in *table 2*. The first case deals with constant speed and variable torque load, second cased deals with variable speed and torque load. The simulation results are represented under the 2nd design scenario (C2), like variable speed and torque load.

Table 1: Specification considered for PMSM modeling

Parameters	Values taken
Stator Resistance (Rs), dq-axis inductance (L_d, L_q)	0.268 Ω, 2.2 mH, 2.2 mH,
Flux Linkage (λ_f), Inertia (J), Friction Factor (B)	0.123 V.s, 0.0146 Kg.m2, 1.66 Ns/m
No. of pole pairs (N_p), Rated Torque (T_r), Rated speed (N_r)	4, 0-14 Nm, 4500 rpm
The inverter Switching frequency (f_s)	5 kHz,
PID Controller Gains: K_p, K_i,	1.2, 0.4

Table 2: Design scenarios used for PMSM system using load torque observers

Design scenarios	Reference speed (W_{ref})	Torque Load (T_l)
C1	1200	1-5-10-5-1
C2	100-500-1000-500-100	1-5-10-5-1

The speed and load torque (Reference and Actual) for the NFC-based PMSM system are illustrated in *figure 3*. The reference and actual speed are shown in *figure 3(a)*. The variable reference speed is considered, and the PMSM model produces the actual (measured) speed with minor differences. The reference and measured (actual) load torque is shown in *figure 3(b)*. The actual torque load is obtained without observers, meaning no observers (NO). The measured torque load produces a considerable error (like spikes), while the reference torque load changes concerning time. So, there is a need for estimators or observers to estimate the actual load torque and also compensate for the noise.

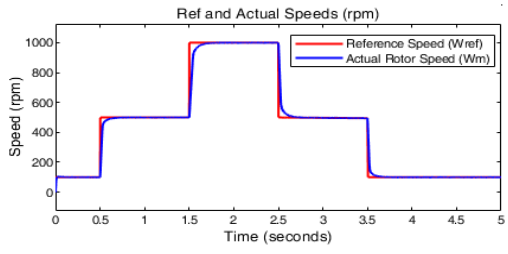

(a)

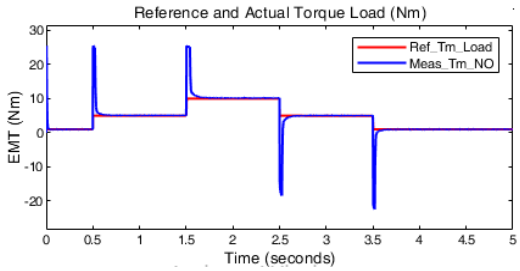

(b)

Figure 3: Speed and Load torque for NFC-based PMSM system. It contains (a) Reference and Actual Speed; (b) Reference and Actual Torque load

FOREX Publication
Open Access | Rapid and quality publishing
International Journal of Electrical and Electronics Research (IJEER)
Research Article | Volume 11, Issue 1 | Pages 01-09 | e-ISSN: 2347-470X

The three-phase stator current for NFC-based PMSM system is represented in *figure 4*. When the reference torque load changes, the three-phase current also changes its phases. The speed error input, NFC output, and *dq*-axis currents for the NFC-based PMSM system are represented in *figure 5*. The speed error is input to NFC, and its output response is shown in *figure 5(a)*. The NFC improves the dynamic response of the error signal and considers a q-axis reference current (I_{qref}). The *dq*-axis reference and measured current are shown in *figure 5(b)*. The measured *dq*-axes current is produced only after performing the transformation (*abc* to *dq*) using I_{abc} and theta.

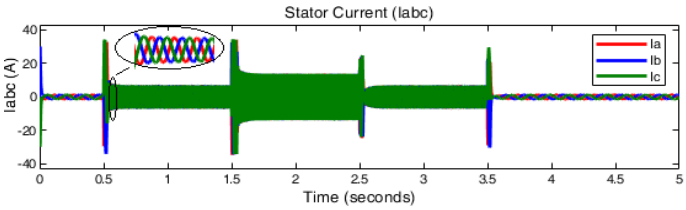

Figure 4: Three Phase stator current for NFC-based PMSM system

The load torque and speed estimation using observers for the NFC-based PMSM system is illustrated in *figure 6*. The load-torque estimate is shown in *figure 6(a)*, and Discrete KFO produces a better response than other observers (DLO and KFO). The overshoot time is more in DLO and KFO than DKFO using NFC for the PMSM system. *Figure 6(b)* shows the speed estimation using three load observers. All three estimated observers are at a similar speed with the minimal difference compared to the reference speed.

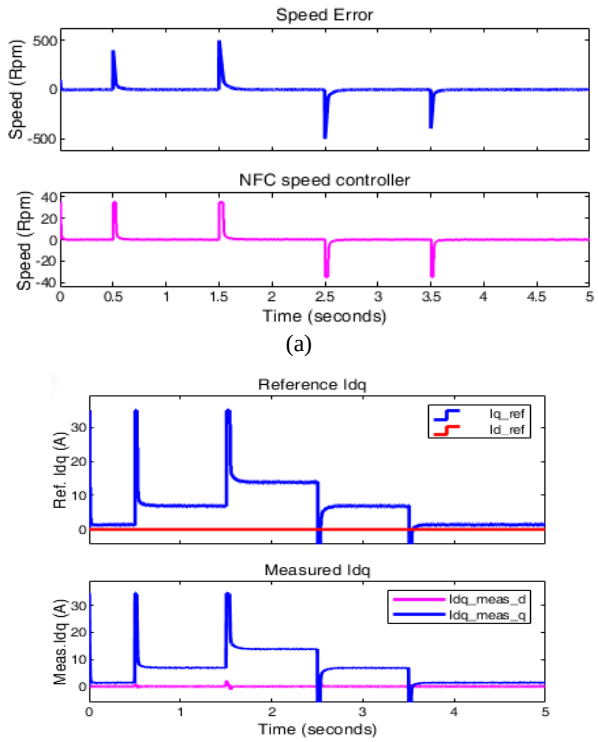

Figure 5: Controller and *dq*-current results for NFC-based PMSM system. It contains (a) Speed Error and NFC output; (b) Reference and measured *dq*-Current

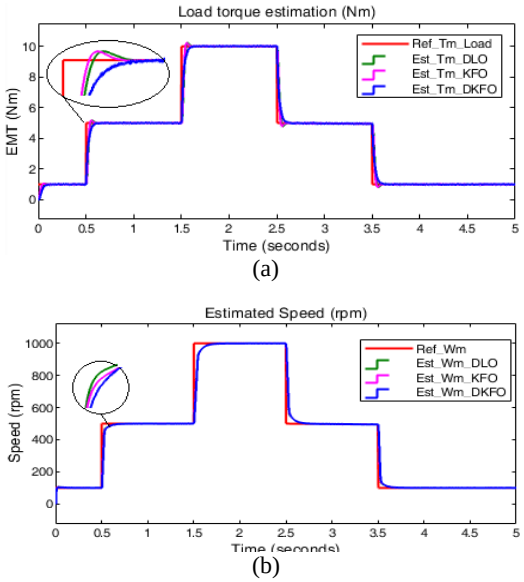

Figure 6: Performance estimation using observers for NFC-based PMSM system. It contains (a) Load Torque estimation; (b) Speed estimation

The average error that occurred during load torque and speed estimation for the NFC-based PMSM system is represented in *figure 7*. The average load torque error is estimated by considering the difference between reference torque load and estimated torque using observers. The DKFO generates a lower average error for load torque during load-toque estimation than DLO and KFO. In contrast, the error that occurred in Speed estimation is shown in *figure 7(b)*. The average speed error is estimated by considering the difference between reference speed and estimated speed using observers. The DKFO provides less average speed error during speed estimation than DLO and KFO. The angle (position) estimation using observers for the NFC-based PMSM system is illustrated in *figure 8*.

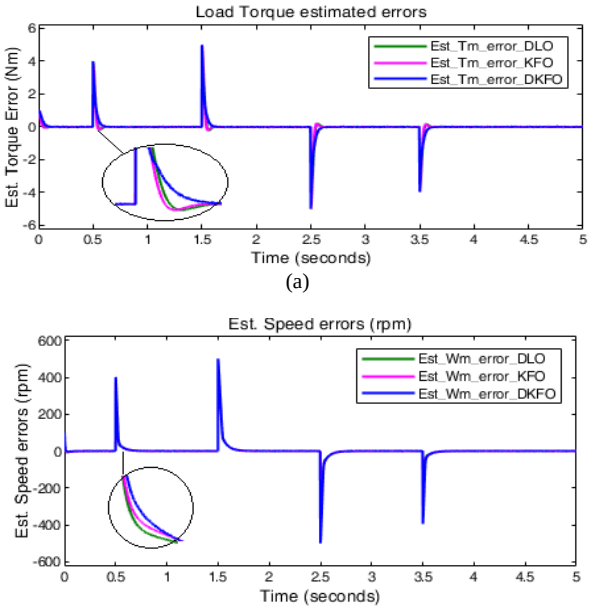

Figure 7: An average error occurred in performance estimation for NFC-based PMSM system. It contains (a) Error occurred in Load Torque estimation; (b) Error occurred in Speed estimation

FOREX Publication
Open Access | Rapid and quality publishing
International Journal of Electrical and Electronics Research (IJEER)
Research Article | Volume 11, Issue 1 | Pages 01-09 | e-ISSN: 2347-470X

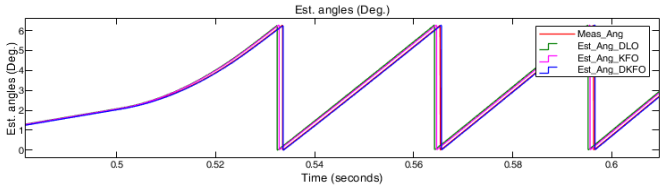

Figure 8: Angle estimation using observers for NFC-based PMSM system

The measured angle is obtained after modeling the PMSM system. The estimated angles are calculated during load-torque estimation. The KFO and DKFO provide better-estimated angles than DLO with minimal error compared to measured angles.

5. DISCUSSION

The average load-toque error estimation for the PMSM system is tabulated in *table 3*. The NFC-based PMSM system is compared with PI Controller and FLC using different observers concerning the load-torque error estimation. The FLC is designed individually for both design scenarios and is used here only for comparison. The designed FLC has 49 design rule sets and seven membership functions.

Table 3: Average Load-toque error estimation for PMSM system

Load-toque error estimation (Nm)			
Designs	**PID**	**FLC**	**NFC**
No Observer			
C1	0.5674	0.569	0.56
C2	0.0997	0.0957	0.0095
DLO			
C1	1.37E-04	2.36E-04	8.65E-05
C2	0.0012	0.001024	0.0016
KFO			
C1	6.62E-04	7.52E-04	4.47E-04
C2	6.71E-04	6.19E-04	0.00105976
DKFO			
C1	0.0039	0.00358	0.0034
C2	0.0049	0.0048	0.0046

The NFC-based PMSM system using DLO (C1) utilizes less load-toque error in 36.8 % than the PI controller and 63.3 % than FLC. Similarly, The NFC-based PMSM system using KFO (C1) utilizes less load-toque error in 32.47 % than the PI controller and 40.5% than FLC. The NFC-based PMSM system using DKFO (C1) utilizes less load-toque error in terms of 12.8 % than the PI controller and 5 % than FLC. When No observer is used in the PMSM system, it gives more than 90% load–torque error compared to all three observers and controllers. The average error for load-torque estimators for the PMSM system is represented in *figure 9*.

The average speed and angle error estimations for the PMSM system using different load observers and controller is tabulated in *table 4*. The NFC-based PMSM system using DLO (C1) utilizes less speed error in 16.45 % than the PI controller and 13.13 % than FLC. Similarly, The NFC-based PMSM system using KFO (C1) utilizes less speed error in terms of 16.48 % than PI controller and 13.1 % than FLC. The NFC-based PMSM system using DKFO (C1) utilizes less speed error in 16.45 % than the PI controller and 13.05 % than FLC. In contrast, The NFC-based PMSM system using DLO (C1) utilizes less angle error in terms of 38.3 % than the PI controller and 34.16 % than FLC. Similarly, The NFC-based PMSM system using KFO (C1) utilizes less angle error in terms of 19.39 % than the PI controller and 30.14 % than FLC. The NFC-based PMSM system using DKFO (C1) utilizes less angle error in terms of 97.3 % than the PI controller and 97.25 % than FLC.

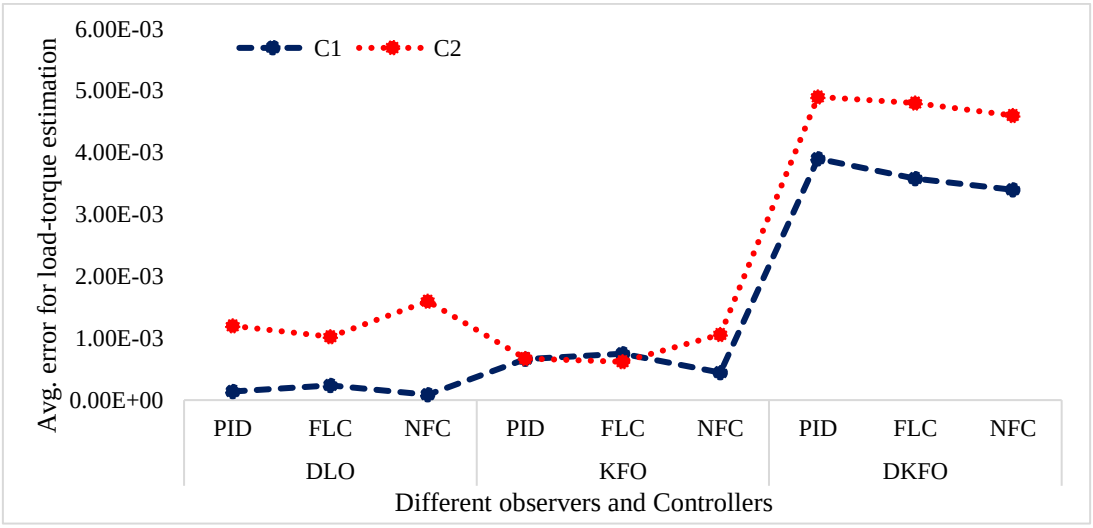

Figure 9: Average error for load-torque estimators for PMSM system

FOREX Publication
Open Access | Rapid and quality publishing
International Journal of Electrical and Electronics Research (IJEER)
Research Article | Volume 11, Issue 1 | Pages 01-09 | e-ISSN: 2347-470X

Table 4: Average speed and angle error estimations for PMSM system

Designs	Wm error estimation (rpm)			Avg. Angle error estimation (deg)		
	PID	FLC	NFC	PID	FLC	NFC
DLO						
C1	14.411	13.86	12.04	0.03	0.0281	0.0185
C2	1.0841	0.859	0.847	0.041	0.00286	0.0185
KFO						
C1	14.417	13.87	12.04	0.0299	0.0345	0.0241
C2	1.0909	0.864	0.834	0.004	0.00499	0.00333
DKFO						
C1	14.436	13.88	12.06	0.1464	0.1406	0.00386
C2	1.1047	0.876	0.869	0.0548	0.0591	0.0541

The estimated errors comparison of the proposed design with existing approaches are tabulated in *table 5*. The reference speed, Load torque, LTO approach, and estimated errors (torque and position) parameters are considered for performance comparison.

Table 5: Comparison of proposed works with existing works [9-10]

Designs	Speed (RPM)	Load Torque (Nm)	LTO	Estimated errors
Estimated Torque error				
Ref [9]	1000	50	MLPF	0.1224
Ref [9]	600	50	MLPF & RVC	0.02
This work	500-1000	5 to 50	DLO	0.000902
			KFO	0.000106
			DKFO	0.00453
Estimated Position Error				
Ref [10]	150	1 to 5	DOBC	0.168
This work	100-500	1 to 10	DKFO	0.0618

The modified low-pass-filter (MLPF) integrated MLPF and reference voltage correction (RVF) approaches were used to estimate the load-torque error in IPMSM [9]. The MLPF and integrated MLPF-VRC obtain the load-torque error of 0.1224 and 0.02 at 50 Nm load torque. The proposed work using LTOs (DLO/KFO/DKFO) reduces the estimated load torque error than existing works [9]. Similarly, the PMSM drive using disturbance observer-based control (DOBC) mechanism [10] is used to estimate the position error and achieves 0.168. The proposed PMSM system using DKFO improves the estimated position error overhead by 63.21% compared to the DOBC-based PMSM system [10].

6. CONCLUSION AND FUTURE WORK

The NFC-based PMSM system is modeled using different load-torque observers in this manuscript. The load-torque observers provide the feed-forward compensation feature to estimate the performance metrics. The NFC-based PMSM system contains NFC based Speed controller, a PI-based current controller with back EMF decoupling, Vector transformations, and different load observers. The PMSM model provides the measured (actual) speed, torque, position, and three-phase and dq stator currents. The measured torque and speed are added with noise and compensated using load observers. The load observers provide the compensated q-axis current to the q-axis-based current controller. The variable speed and torque scenarios discuss the simulation results, including speed, torque, three-phase, and dq-currents. The work estimated the load-toque, speed, position, and error using different load observers and compared them with a PI//FLC-based PMSM system with better performance improvements. In the future, analyze the dynamic responses of the estimated load torque and speed. The proposed PMSM system will be analyzed in a hardware environment to realize real-time performance metrics.

REFERENCES

[1] Ugale, Rajaram Tukaram, Bhalchandra Nemichand Chaudhari, and Ashutosh Pramanik. "Overview of research evolution in line start permanent magnet synchronous motors." IET Electric Power Applications, Vol. 8, no. 4, pp. 141-154, 2014, doi: 10.1049/iet-epa.2013.0241.

[2] Nobahari, Amin, Mehdi Aliahmadi, and Jawad Faiz. "Performance modifications and design aspects of rotating flux switching permanent magnet machines: a review." IET Electric Power Applications, vol. 14, no. 1, pp. 1-15, 2020, doi: 10.1049/iet-epa.2019.0339.

[3] Chen, Hao, Yuefei Zuo, K. T. Chau, Wenxiang Zhao, and Christopher HT Lee. "Modern electric machines and drives for wind power generation: A review of opportunities and challenges." IET Renewable Power Generation, vol. 15, no. 9, pp.1864-1887, 2021,doi: 10.1049/rpg2.12114.

[4] Ahn, Hanwoong, Hyunjong Park, Changhyun Kim, and Hyungwoo Lee. "A Review of State-of-the-art Techniques for PMSM Parameter Identification." Journal of Electrical Engineering & Technology, vol. 15, no. 3 pp. 1177-1187, 2020, doi: 10.1007/s42835-020-00398-6.

[5] Rafaq, Muhammad Saad, and Jin-Woo Jung. "A comprehensive review of state-of-the-art parameter estimation techniques for permanent magnet synchronous motors in wide speed range." IEEE Transactions on Industrial Informatics, vol. 16, no. 7, pp. 4747-4758, 2019, doi: 10.1109/TII.2019.2944413.

[6] Janiszewski, Dariusz. "Load torque estimation in sensorless PMSM drive using Unscented Kalman Filter." In 2011 IEEE International Symposium on Industrial Electronics, pp. 643-648. IEEE, 2011.doi: 10.1109/ISIE.2011.5984233.

[7] Sim, Hyun-Woo, June-Seok Lee, and Kyo-Beum Lee. "Online parameter estimation of interior permanent magnet synchronous motor using an extended Kalman filter." Journal of Electrical Engineering and

Technology, vol. 9, no. 2, pp. 600-608, 2014, doi: 10.5370/JEET.2014.9.2.600.

[8] Tseng, Shao-Kai, Tian-Hua Liu, and Jui-Ling Chen. "Implementation of a sensorless interior permanent magnet synchronous drive based on current deviations of pulse-width modulation switching." IET Electric Power Applications, vol. 9, no. 2, pp. 95-106, 2015, doi: 10.1049/iet-epa.2013.0340.

[9] Wu, Zhihong, Ke Lu, and Yuan Zhu. "A practical torque estimation method for interior permanent magnet synchronous machine in electric vehicles." Plos one, vol. 10, no. 6, pp. e0130923, 2015, doi: 10.1371/journal.pone.0130923.

[10] Xiaoquan, Lu, Lin Heyun, and Han Junlin. "Load disturbance observer-based control method for sensorless PMSM drive." IET Electric Power Applications, vol. 10, no. 8, pp. 735-743, 2016, doi: 10.1049/iet-epa.2015.0550.

[11] Zhao, Kai-Hui, Chang-Fan Zhang, Jing He, Xiang-Fei Li, Jiang-Hua Feng, Jian-Hua Liu, and Tao Li. "Accurate torque-sensorless control approach for interior permanent-magnet synchronous machine based on cascaded sliding mode observer." The Journal of Engineering, vol. 2017, no. 7, pp. 376-384, 2017, doi: 10.1049/joe.2017.0160.

[12] Tami, Ramdane, Driss Boutat, Gang Zheng, Frédéric Kratz, and Rachid El Gouri. "Rotor speed, load torque and parameters estimations of a permanent magnet synchronous motor using extended observer forms." IET Control Theory & Applications, vol. 11, no. 9, pp. 1485-1492, 2017, doi: 10.1049/iet-cta.2016.0226.

[13] O. Asseu, P. Yoboue, A. Konate and M. Diaby. An Extended Kalman Filter Algorithm for a PMSM: Experimental Results. Asian Journal of Applied Sciences, vol. 10, pp. 32-38, 2017, doi: 10.3923/ajaps.2017.32.38.

[14] Yang, Haitao, Yongchang Zhang, Jiejunyi Liang, Bo Xia, Paul D. Walker, and Nong Zhang. "Deadbeat control based on a multipurpose disturbance observer for permanent magnet synchronous motors." IET Electric Power Applications, vol. 12, no. 5, pp. 708-716, 2018, doi: 10.1049/iet-epa.2017.0678.

[15] Tian, Gao, Yang Yan, Wang Jun, Zhou Yu Ru, and Zhao Xiao Peng. "Rotor position estimation of sensorless PMSM based on extended Kalman filter." In 2018 IEEE International Conference on Mechatronics, Robotics and Automation (ICMRA), pp. 12-16. IEEE, 2018, doi: 10.1109/ICMRA.2018.8490558.

[16] Sun, Xiaofei, Haisheng Yu, Jinpeng Yu, and Xudong Liu. "Design and implementation of a novel adaptive backstepping control scheme for a PMSM with unknown load torque." IET Electric Power Applications, vol. 13, no. 4, pp. 445-455, 2019, doi: 10.1049/iet-epa.2018.5656.

[17] Zhang, Hang, Weiguo Liu, Zhe Chen, Ningfei Jiao, and Dongdong Zhao. "Comparison analysis of low-switching-frequency-based IPMSM sensorless drives considering regulators, observer and inverter non-linearity." IET Electric Power Applications, vol. 13, no. 7, pp. 1022-1031, 2019, doi: 10.1049/iet-epa.2019.0007.

[18] Xu, Yongxiang, Minghui Wang, Wentao Zhang, and Jibin Zou. "Sliding mode observer for sensorless control of surface permanent magnet synchronous motor equipped with LC filter." IET Power Electronics, vol. 12, no. 4, pp. 686-692, 2019, doi: 10.1049/iet-pel.2018.5218.

[19] Eldigair, Yousif, Abdul R. Beig, and Jamal Alsawalhi. "Sensorless DTSMC of a three-level VSI fed PMSM drive." IET Power Electronics, vol. 13, no. 4, pp. 788-797, 2020, doi: 10.1049/iet-pel.2018.5523.

[20] Niewiara, Ł. J., T. Tarczewski, and L. M. Grzesiak. "Application of extended Kalman filter for estimation of periodic disturbance and velocity ripple reduction in PMSM drive." Bulletin of the Polish Academy of Sciences. Technical Sciences, vol. 68, no. 5, 2020, doi: 10.24425/bpasts.2020.134649.

[21] Niedermayr, Philipp, Luigi Alberti, Silverio Bolognani, and Reiner Abl. "Implementation and experimental validation of ultra-high speed PMSM sensor-less control by means of extended Kalman filter." IEEE Journal of Emerging and Selected Topics in Power Electronics, 2020, doi: 10.1109/JESTPE.2020.3041026.

[22] Ge, Yang, Lihui Yang, and Xikui Ma. "Sensorless control of PMSM using generalized extended state observer and adaptive resistance estimation." IET Electric Power Applications, vol. 14, no. 11, pp. 2062-2073, 2020, doi: 10.1049/iet-epa.2019.0729.

[23] He, Wenyun, Xiang Wu, Junlei Chen, and Yu Wang. "Comparative study of sensorless control of Permanent magnet synchronous motor realized by the sliding-mode observer." IET Power Electronics, vol. 13, no. 6, pp. 1191-1199, 2020, doi: 10.1049/iet-pel.2019.1153.

[24] Chung-Hui Lee, Hui-Seong Shin and Ki-Chan Kim (2022), Analysis of Interior Permanent Magnet Synchronous Motor according to Winding Method. IJEER 10(2), 207-213. DOI: 10.37391/IJEER.100227.

[25] Wang, Yongwei, Jingbo Wu, Zhijun Guo, Chengwei Xie, Junjie Liu, Xin Jin, and Zhifu Wang. "Fuzzy adaptive super-twisting algorithm based sliding-mode observer for sensorless control of permanent magnet synchronous motor." The Journal of Engineering, vol. 2021, no. 12, pp. 788-799, 2021, doi: 10.1049/tje2.12076.

[26] Arun Eldho Alia and F. T. Josh (2022), Design Analysis of SSD Optimized Speed Controller for BLDC Motor. IJEER 10(3), 529-535. DOI: 10.37391/IJEER.100321.

[27] C. L. Phillips, and R. D. Harbor, Feedback Control Systems 4th Edition. New Jersey: Prentice Hall, 2000, ISBN: 0-13-949090-6.

[28] Dan Simon, Optimal State Estimation 2006, John Wiley and Sons, Inc. ISBN: 13-978-0-471-70858-2.